Journal of Materials Chemistry A

PAPER

View Article Online
View Journal | View Issue

Cite this: J. Mater. Chem. A, 2017, 5, 3541

Rapid preparation of $In_xCo_4Sb_{12}$ with a record-breaking $ZT = 1.5$: the role of the In overfilling fraction limit and Sb overstoichiometry

V. V. Khovaylo,*[a] T. A. Korolkov,[a] A. I. Voronin,[ab] M. V. Gorshenkov[a] and A. T. Burkov[c]

Received 19th October 2016
Accepted 11th January 2017

DOI: 10.1039/c6ta09092c

www.rsc.org/MaterialsA

Samples of indium-filled $In_xCo_4Sb_{12}$ skutterudite were successfully synthesized by conventional induction melting without the use of evacuated quartz ampoules. Addition of In above the filling fraction limit ($x \approx 0.22$) and adjustment of Sb excess in the induction-melted $In_xCo_4Sb_{12}$ ingots allowed us to suppress formation of the unwanted $CoSb_2$ phase in the sintered samples and effectively control the amount of the InSb impurity phase which precipitated in nanometer-sized regions along the grain boundaries of the main skutterudite phase. Measurements of the Seebeck coefficient, electrical conductivity and thermal conductivity of the $In_xCo_4Sb_{12}$ samples with nominal In contents $x = 0.2$, 0.6, and 1.0 revealed a simultaneous increase in the electrical conductivity and decrease in the thermal conductivity. This results in the record value of the thermoelectric figure of merit $ZT \approx 1.5$ for single-filled skutterudites which was attained in the $In_1Co_4Sb_{12}$ sample at 725 K.

Introduction

Thermoelectric materials (TEs) have attracted much attention due to their environment-friendly applications in power generation and refrigeration.[1,2] Among TEs, skutterudite antimonides have been considered as one of the best materials for applications at intermediate temperatures.[3–5] The specific feature of skutterudites is the existence of interstitial voids in the body-centered cubic (bcc) crystal structure (space group $Im\bar{3}$). Filling the voids by guest atoms allows one to greatly reduce the thermal conductivity of skutterudites which in turn significantly enhances the dimensionless thermoelectric figure of merit ZT defined as $ZT = \sigma S^2 T/\kappa$, where σ is the electrical conductivity, S is the Seebeck coefficient, T is the absolute temperature, and κ is the total thermal conductivity. Since the guest atoms strongly reduce the thermal conductivity due to the "rattling effect"[6,7] and, at the same time, can also optimize the carrier concentration, filled skutterudites have been considered as a good example for the support of Slack's "phonon glass – electron crystal" concept.[8]

For undoped Co_4Sb_{12}, a ZT above unity has been reported for the case of filling by In ($ZT_{max} = 1.2$),[3,9–11] Yb ($ZT_{max} \sim 1.4$),[12–16] Ba ($ZT_{max} = 1.1$),[17] Na ($ZT_{max} = 1.25$),[18] and Li (under high-pressure sintering conditions, $ZT_{max} = 1.3$).[19] Double and triple filling of Co_4Sb_{12}-based skutterudites has been found to be a very effective approach toward reaching even a higher ZT in these materials due to introduction of several rattling modes into the host material[20] and optimization of the electrical transport properties by adjusting the filling fractions of the guest atoms.[21] Utilization of this approach has allowed one to increase the ZT up to 1.43 in double-filled[3,22–24] and up to 1.7 in triple-filled Co_4Sb_{12}-based skutterudites.[25–30] Moreover, it has been reported that the ZT approaches 2 in multi-filled skutterudites subjected to severe plastic deformation.[31–33]

Due to an intricate picture of phase equilibria in filled antimony-based skutterudites, precipitate phases are usually presented alongside the main phase. For instance, InSb and $CoSb_2$ impurity phases as well as elemental antimony have been frequently observed in $In_yCo_4Sb_{12}$ skutterudites.[11,13,34–39] Judging by a number of reports,[36,40–42] the InSb impurity phase formed as *in situ* nanoinclusions can considerably enhance the thermoelectric performance of the host phase due to simultaneous enhancement of its electrical transport properties and suppression of its thermal conductivity. It should be noted however that the concentration of InSb nanoinclusions in $In_yCo_4Sb_{12}$ is limited because the formation of the InSb phase leads to a Sb deficiency which is accompanied by the appearance of the $CoSb_2$ phase.

Other critical issue in the large-scale production of filled Co_4Sb_{12}-based skutterudites is their preparation methods. Several rapid preparation methods, such as melt-spinning,[13,14] mechanical alloying[43] or microwave sintering,[44] have been proposed for the fabrication of antimony-based skutterudites. Traditional preparation methods consist of several steps, such as melting in a sealed quartz ampoule followed by a long-time annealing, grinding the ingot into powder and its consolidation by spark plasma sintering or hot pressing techniques.[35]

[a]National University of Science and Technology "MISiS", Moscow 119049, Russia. E-mail: khovaylo@misis.ru
[b]National Research South Ural State University, Chelyabinsk 454080, Russia
[c]A.F. Ioffe Physical-Technical Institute, St. Petersburg 194021, Russia

Because of the high volatility of Sb, it is a common practice to use sealed quartz ampoules in the fabrication process of antimony-based skutterudites which is inconvenient for the large-scale production of these materials. Here we show that $In_xCo_4Sb_{12}$ skutterudites can be prepared in large quantities by a conventional induction melting in ordinary Al_2O_3 crucibles. We also show that the concentration of InSb nanoinclusions in $In_xCo_4Sb_{12}$ skutterudites can be effectively controlled by the adjustment of Sb excess and addition of In above the filling fraction limit which allowed us to reach the record-breaking value of the ZT in a single-filled $In_xCo_4Sb_{12}$ skutterudite with a nominal In content $x = 1$.

Experimental

Ingots of $In_xCo_4Sb_{12}$ skutterudites with nominal In contents $x =$ 0.2, 0.6, and 1.0 were synthesized in a rapid mode by the conventional induction melting technique from elemental In (99.9%, chunks), Co (99.9%, flakes), and Sb (99.9995%, chunks). Weighed in desired proportions In, Co, and Sb were melted in an Al_2O_3 crucible for 2 minutes and quenched in a cooper mold of a cylindrical form. After that, the ingots were annealed at 973 K for 5 hours to improve the chemical homogeneity. The annealed ingots were ground into fine powders by using a Fritsch planetary mill (Pulverisette 7 premium line) using zirconium oxide balls (ϕ 10 mm in diameter) for 5 hours at a revolving speed of 700 rpm. All work with the powders was performed under an Ar atmosphere in a glovebox. The powder was consolidated by using a spark plasma sintering (SPS) Labox 650 machine at 900 K under a pressure of 50 MPa for 10 minutes. The consolidated pellets were cut into a disc (ϕ 12 × 2 mm^3) for thermal conductivity measurements and a slice (2 × 10 × 0.5 mm^3) for electrical transport and Seebeck coefficient measurements.

Room-temperature X-ray diffraction (XRD) patterns were collected by using a SmartLab Rigaku diffractometer with CuKα radiation ($\lambda = 1.57$ Å) from $2\theta = 10°$ to $2\theta = 80°$ with a step of 0.01°. The structure of the samples was characterized by scanning electron microscopy (SEM, JEOL 6700) in backscattered electron signals. Transmission electron microscopy (TEM) investigations were done on a JEOL JEM1400 microscope operating at 120 kV. Transparent foils for the TEM studies were prepared by Ar ion milling at 5 keV energy at an angle of 3° and final fine milling at 2 keV, 2° glancing angle. The Seebeck coefficient S and electrical conductivity σ were measured independently at the NUST "MISiS" by a 4-probe method using a high-temperature transport measurement system (Cryotel, Co.) with an accuracy of 8% for $S(T)$ and 5% for $\sigma(T)$ and at the Ioffe Institute using the standard DC 4-point configuration for the electrical conductivity measurements and the differential method for the Seebeck coefficient measurements.[45] The thermal conductivity κ was calculated from the thermal diffusivity D_t, density ρ and specific heat C_p. The thermal diffusivity was measured independently at the NUST "MISiS" by a laser flash method (Netzsch LFA 447) and at ITMO University by using a Xenon flash apparatus Linseis XFA 500. The density of the samples was measured by the Archimedes method. The specific heat C_p measured by the differential scanning calorimetry method (Netzsch DSC 204 F1) was found to depend weakly on the temperature and does not exceed 0.22 J g^{-1} K^{-1}.

Results and discussion

Structural characterization

The powder X-ray diffraction measurements revealed (Fig. 1) that all the $In_xCo_4Sb_{12}$ ($x = 0.2$, 0.6, 1.0) samples crystallize in a cubic structure (space group $Im\bar{3}$). Analysis of the XRD data indicates that the crystal lattice parameter a slightly increases from $a =$ 0.9041(3) nm to $a = 0.9056(8)$ nm as the nominal In content increases from $x = 0.2$ to $x = 1.0$ which is in good agreement with the lattice parameter reported in ref. 38. Considering that the previous reports[9,34] showed that the lattice parameter of $In_yCo_4Sb_{12}$ increases and saturates for the In content corresponding to the filling fraction limit, it can be suggested that the In filling fraction limit (~0.22) is reached neither in $x = 0.2$ nor in the $x =$ 0.6 sample. The results of the EDX analysis confirmed this suggestion, *e.g.*, the real chemical composition of the $x = 0.6$ sample was found to be $In_{0.1}Co_4Sb_{12}$. This implies that some of the In atoms in the $x = 0.2$ and $x = 0.6$ samples participated in the formation of the InSb phase or can be presented in the samples in the elemental form. Since no reflections corresponding to a foreign phase were observed in the corresponding X-ray diffraction patterns (Fig. 1), the amount of this phase should be below the XRD resolution limit. Also, taking into account the high vapor pressure of In, it is reasonable to consider that some indium was lost during the induction melting of the ingots.

The impurity InSb phase is clearly observed in the XRD patterns of the $x = 0.6$ and $x = 1.0$ samples (Fig. 1). According to the SEM characterization of this sample (Fig. 2), the InSb impurity phase is mainly distributed in nanometer-sized regions along the grain boundaries and in the main skutterudite phase. The real chemical composition of the main skutterudite phase in the $x = 1.0$ sample was determined to be $In_{0.19}Co_4Sb_{12}$, *i.e.*, with the In content close to the filling fraction

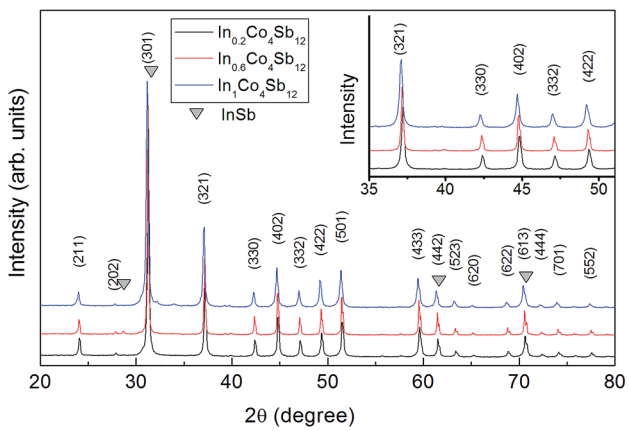

Fig. 1 XRD patterns of $In_xCo_4Sb_{12}$ (from bottom to top: $x = 0.2$, 0.6, 1.0). The inset: a part of the XRD patterns showing a shift in the position of X-ray reflections.

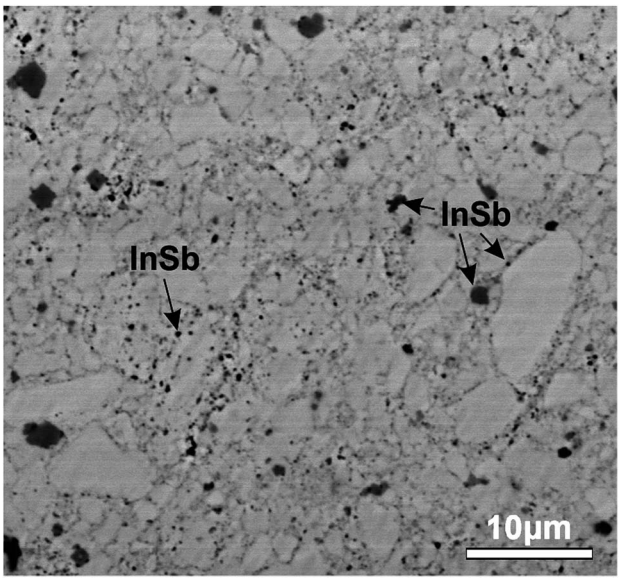

Fig. 2 SEM image of the SPS-sintered $In_xCo_4Sb_{12}$ sample with $x = 1.0$.

limit.[38,39] The fact that the frequently detected secondary phase of $CoSb_2$ in antimony-based skutterudites[34,35,37,38] is absent in our samples is presumably due to a rather large, ~10 wt%, excess of Sb which was added to the nominal composition before melting the ingots. We suggest that such a Sb excess is sufficient to compensate for Sb lost during the induction melting and to participate in the formation of the InSb phase thus preventing the formation of the unwanted $CoSb_2$ phase. The results of the SEM observations indicated that the samples are well consolidated. This is in accordance with the results of the density measurement which showed that the samples have a density of about 98% of the theoretical one.

Shown in Fig. 3 is an example of TEM images taken for the SPS-sintered samples. The average grain size is about 200 nm which is comparable with that reported for In-doped multifilled

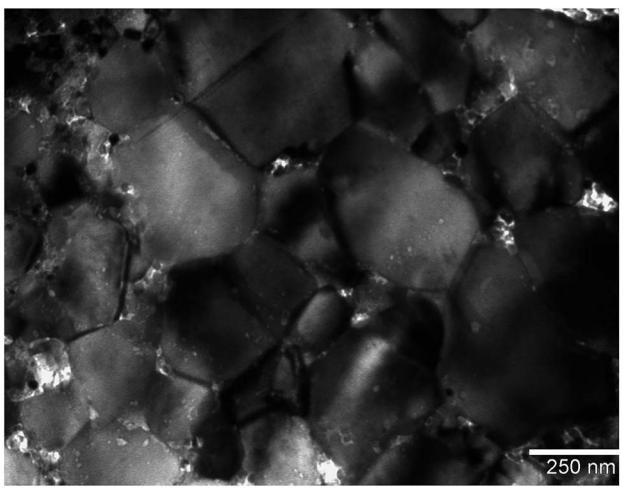

Fig. 3 TEM image of the SPS-sintered $In_xCo_4Sb_{12}$ sample with $x = 1.0$.

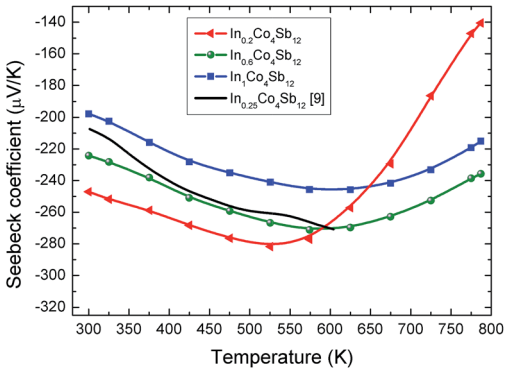

Fig. 4 Temperature dependencies of the Seebeck coefficient S in $In_xCo_4Sb_{12}$ ($x = 0.2$, 0.6, 1.0) samples. Data of the $S(T)$ dependence in $In_yCo_4Sb_{12}$ with the In filling fraction $y = 0.25$ (ref. 9) are shown for comparison.

skutterudites[33] with $ZT = 1.8$ and for SPS-compacted melt-spun ribbons of $Yb_{0.3}Co_4Sb_{12.3}$ with $ZT = 1.3$.[13]

Thermoelectric properties

The temperature dependencies of the Seebeck coefficient and electrical conductivity for the $In_xCo_4Sb_{12}$ ($x = 0.2$, 0.6, 1.0) samples are shown in Fig. 4. All samples have a negative Seebeck coefficient ranging from −200 to −260 μV K^{-1}, indicative of n-type semiconductors. The absolute value of the Seebeck coefficient decreases with increasing x which is common for In-filled skutterudites.[34,35,39] The upturn in $S(T)$ seen near ~580 K is consistent with the data reported for a series of $In_yCo_4Sb_{12}$ samples by Li *et al.*[37] and Visnow *et al.*[39] and can be ascribed to the onset of bipolar conduction which involves thermal excitations of electrons over the band gap and resulting holes in the valence band. It is interesting to note that the behavior of $S(T)$ in our sample with $x = 0.2$ resembles that reported in ref. 35 and 37 for $In_yCo_4Sb_{12}$ with a low ($y = 0.05$) indium content. Recalling that the real In content in our samples is significantly smaller than the nominal one, the similarity of $S(T)$ seen in our $x = 0.2$ sample and

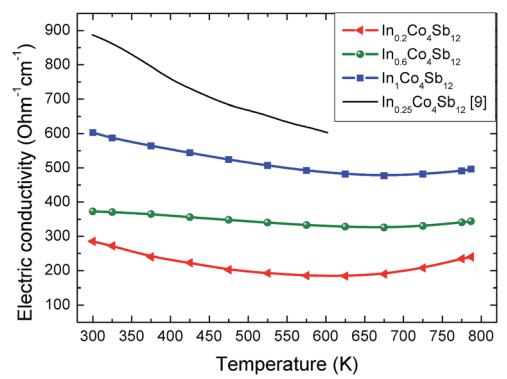

Fig. 5 Temperature dependencies of the electrical conductivity σ in $In_xCo_4Sb_{12}$ ($x = 0.2$, 0.6, 1.0) samples. Data of the $\sigma(T)$ dependence in $In_yCo_4Sb_{12}$ with the In filling fraction $y = 0.25$ (ref. 9) are shown for comparison.

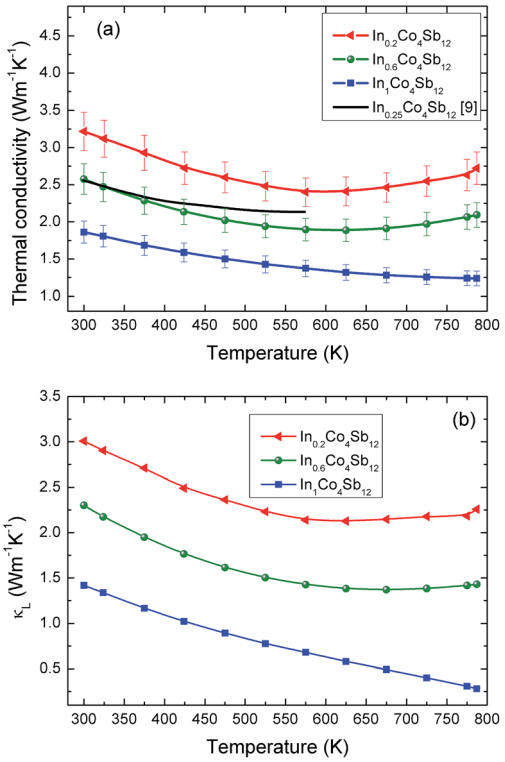

Fig. 6 Temperature dependencies of the total thermal conductivity κ (a) and lattice thermal conductivity κ_L (b) in $In_xCo_4Sb_{12}$ ($x = 0.2, 0.6, 1.0$) samples. Data of the $\kappa(T)$ dependence in $In_yCo_4Sb_{12}$ with the In filling fraction $y = 0.25$ (ref. 9) are shown for comparison.

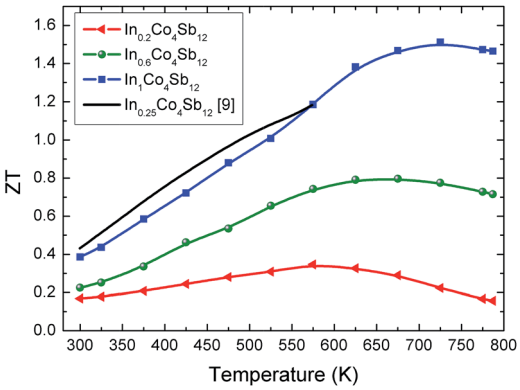

Fig. 7 Figure of merit ZT as a function of temperature in $In_xCo_4Sb_{12}$ ($x = 0.2, 0.6, 1.0$) samples. Data of the ZT dependence in $In_yCo_4Sb_{12}$ with the In filling fraction $y = 0.25$ (ref. 9) are shown for comparison.

in the sample with $y = 0.05$ (ref. 35 and 37) can be linked to the dependence of the band gap width on the indium filling fraction.

The electrical conductivity measurements show (Fig. 5) that σ increases with increasing In content which suggests that some of the indium acts as an n-type dopant to increase the carrier concentration. As expected, the highest electrical conductivity is obtained for the sample with the largest nominal In content, $x = 1.0$. The decrease of σ with increasing temperature is indicative of heavily doped semiconductors and was previously reported for In-filled skutterudites.[9,34,35,39] The upturn of the electrical conductivity which is clearly seen in the $x = 0.2$ sample at $T \sim 600$ K and in the other samples at a higher temperature indicates the onset of intrinsic semiconductor behavior. This is consistent with the literature data[35,39] and our results of the Seebeck coefficient measurements (Fig. 4) which implies that the bipolar conduction is at play at temperatures above 600 K. Considering the absolute value of the electrical resistivity, our data for the $x = 0.2$ sample agree quite well with that reported by Sesselmann *et al.*[35] for $In_yCo_4Sb_{12}$ with a small In filling fraction ($y = 0.05$) (Fig. 5). As for the $x = 0.6$ and $x = 1.0$ samples, their electrical conductivity is generally lower than the value reported in the literature for $In_yCo_4Sb_{12}$ samples with a large In filling fraction.[34,35,39] This can be a consequence of the fine grain structure of our SPS sintered samples (Fig. 3) which enhances the charge carrier scattering.

The temperature dependencies of the total thermal conductivity κ and lattice thermal conductivity κ_L of $In_xCo_4Sb_{12}$ ($x = 0.2, 0.6, 1.0$) are shown in Fig. 6. For the calculation of κ_L we used the Wiedemann–Franz law assuming that the Lorentz number $L_0 = 2.45 \times 10^{-8}$ V^{-2} K^{-2}.[35] The thermal conductivity decreases with increasing temperature. In the $x = 0.2$ and $x = 0.6$ samples κ exhibits an upturn at $T > 600$ K which can be explained in the framework of the bipolar conduction scenario as caused by the enhancement of the electronic thermal conductivity. Decrease of the thermal conductivity with increasing In nominal content is clearly seen (Fig. 6) which unambiguously shows that the indium filling fraction progressively increases from sample to sample. Generally, the thermal conductivity of all our samples is lower than the reported values of κ in samples with a large In filling fraction[34,35,37,39] and is comparable with the thermal conductivity observed in multi-filled skutterudites.[3,31,33] We believe that the suppression of the thermal conductivity in our samples is conditioned by several factors. First, the small grain size (Fig. 3) gives a sizable contribution to phonon scattering processes. Second, the InSb impurity phase whose presence is anticipated in the $x = 0.2$ and $x = 0.6$ samples and clearly seen in the $x = 1.0$ samples (Fig. 1) acts as effective nanoscale phonon scattering centers. Third, adjustment of Sb excess promotes effective formation of the desired InSb nanoinclusions and suppresses appearance of the unwanted $CoSb_2$ impurity phase.

The temperature dependencies of the dimensionless thermoelectric figure of merit ZT for the studied $In_xCo_4Sb_{12}$ samples are shown in Fig. 7. Due to the significant reduction of the thermal conductivity, a considerable enhancement of the ZT is observed for the $x = 0.6$ and $x = 1.0$ samples. The ZT markedly increases with increasing nominal In content and the maximum ZT value of 1.5 was obtained for the $In_1Co_4Sb_{12}$ sample at 725 K.

Conclusions

In conclusion, we have found that Sb overstoichiometry plays a crucial role in the suppression of the unwanted $CoSb_2$ secondary phase. On the other hand, Sb excess combined with the addition of In above the filling limit favors the formation of

InSb nanoscaled precipitates which strongly affect the thermoelectric properties of the samples. Adjustment of the content of the InSb phase allows one to enhance significantly the *ZT* of the system. For the $In_xCo_4Sb_{12}$ sample with the nominal indium content $x = 1.0$, the *ZT* reaches 1.5 at 725 K which is the record value for single-filled skutterudite compounds. Moreover, the proposed method of sample preparation without the use of evacuated quartz ampoules is very convenient for the large-scale production of skutterudites with a high thermoelectric performance.

Acknowledgements

The authors gratefully acknowledge the financial support of the Ministry of Education and Science of the Russian Federation in the framework of Increase Competitiveness Program of NUST "MISiS".

Notes and references

1 W. He, G. Zhang, X. Zhang, J. Ji, G. Li and X. Zhao, *Appl. Energy*, 2015, **143**, 1.
2 W. Liu, Q. Jie, H. S. Kim and Z. Ren, *Acta Mater.*, 2015, **87**, 357.
3 K. Biswas, M. S. Good, K. C. Roberts, M. A. Subramanian and T. J. Hendricks, *J. Mater. Res.*, 2011, **26**, 1827.
4 J. R. Sootsman, D. Y. Chung and M. G. Kanatzidis, *Angew. Chem., Int. Ed.*, 2009, **48**, 8616.
5 M. Rull-Bravo, A. Moure, J. F. Fernández and M. Martín-González, *RSC Adv.*, 2015, **5**, 41653.
6 G. S. Nolas, J. L. Gohn and G. A. Slack, *Phys. Rev. B: Condens. Matter Mater. Phys.*, 1998, **58**, 164.
7 R. P. Herman, R. Jin, W. Schweika, F. Grandjean, D. Mandrus, B. C. Sales and G. J. Long, *Phys. Rev. Lett.*, 2003, **90**, 135505.
8 G. A. Slack, in *CRC Handbook of Thermoelectrics* ed. D. M. Rowe, CRC Press, 1995, ch. 34.
9 T. He, J. Chen, H. D. Rosenfeld and M. A. Subramanian, *Chem. Mater.*, 2006, **18**, 759.
10 J. Leszczynski, V. Da Ros, B. Lenoir, A. Dauscher, C. Candolfi, P. Masschelein, J. Hejtmanek, K. Kutorasinski, J. Tobola, R. I. Smith, C. Stiewe and E. Müller, *J. Phys. D: Appl. Phys.*, 2013, **46**, 495106.
11 Y. Tang, Y. Qiu, L. Xi, X. Shi, W. Zhang, L. Chen, S.-M. Tseng, S.-W. Chen and G. J. Snyder, *Energy Environ. Sci.*, 2014, **7**, 812.
12 H. Li, X. Tang, X. Su and Q. Zhang, *Appl. Phys. Lett.*, 2008, **92**, 202114.
13 H. Li, X. Tang, Q. Zhang and C. Uher, *Appl. Phys. Lett.*, 2008, **93**, 252109.
14 H. Li, X. Tang, X. Su, Q. Zhang and C. Uher, *J. Phys. D: Appl. Phys.*, 2009, **41**, 145409.
15 J. Yang, Q. Hao, H. Wang, Y. C. Lan, Q. Y. He, A. Minnich, D. Z. Wang, J. A. Harriman, V. M. Varki, M. S. Dresselhaus, G. Chen and Z. F. Ren, *Phys. Rev. B: Condens. Matter Mater. Phys.*, 2009, **80**, 115329.
16 T. Dahal, Q. Jie, G. Joshi, S. Chen, C. Guo, Y. Lan and Z. Ren, *Acta Mater.*, 2014, **75**, 316.
17 L. D. Chen, T. Kawahara, X. F. Tang, T. Goto, T. Hirai, J. S. Dyck, W. Chen and C. Uher, *J. Appl. Phys.*, 2001, **90**, 1864.
18 Y. Z. Pei, J. Yang, L. D. Chen, W. Zhang, J. R. Salvador and J. Yang, *Appl. Phys. Lett.*, 2009, **95**, 042101.
19 J. Zhang, B. Xu, L.-M. Wang, D. Yu, J. Yang, F. Yu, Z. Liu, J. He, B. Wen and Y. Tian, *Acta Mater.*, 2012, **60**, 1246.
20 X. Shi, S. Bai, L. Xi, J. Yang, W. Zhang, L. Chen and J. Yang, *J. Mater. Res.*, 2011, **26**, 1745.
21 W. Zhao, P. Wei, Q. Zhang, H. Peng, W. Zhu, D. Tang, J. Yu, H. Zhou, Z. Liu, X. Mu, D. He, J. Li, C. Wang, X. Tang and J. Yang, *Nat. Commun.*, 2015, **6**, 6197.
22 S. Q. Bai, Y. Z. Pei, L. D. Chen, W. Q. Zhang, X. Y. Zhao and J. Yang, *Acta Mater.*, 2009, **57**, 3135.
23 W. Zhao, P. Wei, Q. Zhang, C. Dong, L. Liu and X. Tang, *J. Am. Chem. Soc.*, 2009, **131**, 3713.
24 J. Yu, W.-Y. Zhao, X. Yang, P. Wei, D.-G. Tang and Q.-J. Zhang, *J. Electron. Mater.*, 2012, **41**, 1395.
25 X. Shi, J. Yang, J. R. Salvador, M. Chi, J. Y. Cho, H. Wang, S. Bai, J. Yang, W. Zhang and L. Chen, *J. Am. Chem. Soc.*, 2011, **133**, 7837.
26 J. Graff, S. Zhu, T. Holgate, J. Peng, J. He and T. M. Tritt, *J. Electron. Mater.*, 2011, **40**, 696.
27 G. Rogl, A. Grytsiv, N. Melnychenko-Koblyuk, E. Bauer, S. Laumann and P. Rogl, *J. Phys.: Condens. Matter*, 2011, **23**, 275601.
28 G. Rogl, Z. Aabdin, E. Schafler, J. Horky, D. Setman, M. Zehetbauer, M. Kriegisch, O. Eibl, A. Grytsiv, E. Bauer, M. Reinecker, W. Schranz and P. Rogl, *J. Alloys Compd.*, 2012, **537**, 183.
29 S. Ballikaya, N. Uzar, S. Yildirim, J. R. Salvador and C. Uher, *J. Solid State Chem.*, 2012, **193**, 31.
30 J. Graff, J. He and T. M. Tritt, *Inorganics*, 2014, **2**, 168.
31 G. Rogl, A. Grytsiv, P. Rogl, N. Peranio, E. Bauer, M. Zehetbauer and O. Eibl, *Acta Mater.*, 2014, **63**, 30.
32 G. Rogl, A. Grytsiv, P. Rogl, E. Bauer, M. Hochenhofer, R. Anbalagan, R. C. Mallik and E. Schafler, *Acta Mater.*, 2014, **76**, 434.
33 G. Rogl, A. Grytsiv, K. Yubuta, S. Puchegger, E. Bauer, C. Raju, R. C. Mallik and P. Rogl, *Acta Mater.*, 2015, **95**, 201.
34 R. C. Mallik, C. Stiewe, G. Karpinski, R. Hassdorf and E. Müller, *J. Electron. Mater.*, 2009, **38**, 1337.
35 A. Sesselman, T. Dasgupta, K. Kelm, E. Müller, S. Perlt and S. Zastrow, *J. Mater. Res.*, 2011, **26**, 1820.
36 J. Eilertsen, S. Rouvimov and M. A. Subramanian, *Acta Mater.*, 2012, **60**, 2178.
37 G. Li, K. Kurosaki, Y. Ohishi, H. Muta and S. Yamanaka, *J. Electron. Mater.*, 2013, **42**, 1463.
38 A. Grytsiv, P. Rogl, H. Michor, E. Bauer and G. Giester, *J. Electron. Mater.*, 2013, **42**, 2940.
39 E. Visnow, C. P. Heirich, A. Scmitz, J. de Boor, P. Leidich, B. Klobes, R. P. Hermann, W. E. Müller and W. Tremel, *Inorg. Chem.*, 2015, **54**, 7818.
40 W. J. Xie, J. He, S. Zhu, X. L. Su, S. Y. Wang, T. Holgate, J. W. Graff, V. Ponnambalam, S. J. Poon, X. F. Tang, Q. J. Zhang and T. M. Tritt, *Acta Mater.*, 2010, **58**, 4705.

41 G. Tan, H. Chi, W. Liu, Y. Zheng, X. Tang, J. He and C. Uher, *J. Mater. Chem. C*, 2015, **3**, 8372.
42 S. Choi, K. Kurosaki, A. Harnwunggmoung, Y. Miyazaki, Y. Ohishi, H. Muta and S. Yamanaka, *Jpn. J. Appl. Phys.*, 2015, **54**, 111801.
43 W.-S. Liu, B.-P. Zhang, J.-F. Li, H.-L. Zhang and L.-D. Zhao, *J. Appl. Phys.*, 2007, **102**, 103717.
44 K. Biswas, S. Muir and M. A. Subramanian, *Mater. Res. Bull.*, 2011, **46**, 2288.
45 A. T. Burkov, A. Heinrich, P. P. Konstantinov, T. Nakama and K. Yagasaki, *Meas. Sci. Technol.*, 2001, **12**, 264.